Desalination and Water Treatment
www.deswater.com
doi: 10.1080/19443994.2013.850744

53 (2015) 898–908
January

Taylor & Francis
Taylor & Francis Group

Simulation of the transport phenomenon occurring in membrane pores during vacuum membrane distillation

Li Xin*, Liu Jia, Ren Shuhua

School of Chemical Engineering and Environment, Beijing Institute of Technology, Beijing 100081, China
Tel. +86 68918978; email: klkxlx@163.com

Received 24 January 2013; Accepted 13 September 2013

ABSTRACT

Basic knowledge regarding flow at conventional scales is relatively familiar to us. However, micro-scale flow is distinctly different. To explore the flow characteristics and mass transfer process in a membrane micro pore, a Knudsen-molecular diffusion mechanism with sliding boundary condition is used to simulate the treatment of ethyl acetate solution using vacuum membrane distillation. The diffusion coefficient is expressed by the Knudsen diffusion coefficient and molecular diffusion coefficient. The simulation results are consistent with the experimental data. The flow fields in the membrane pore are obtained, and the effects of the membrane structure parameters on the membrane pore separation performance are investigated. The results show that the increase in the porosity and pore diameter can enhance the membrane flux and increase the tortuosity and pore length against permeate flux. The optimal choice of the separation factors is presented as a function of the increase in the porosity, pore diameter, and tortuosity. Pore length does not enhance the membrane separation performance. The simulation of the phenomenon occurring in membrane pores should contribute to appropriate membrane preparation and improve membrane separation performance.

Keywords: Vacuum membrane distillation; Ethyl acetate solution; Numerical simulation; Membrane pore

1. Introduction

The rapid development of industry has led to increased wastewater pollution in the form of volatile organic compounds (VOCs). Thus, it is an important task for us to treat the VOCs produced by wastewater. Compared to traditional methods used to treat VOC pollutants, membrane distillation (MD) is becoming a promising separation method due to its advantages of energy saving and environmental friendliness, i.e. in the range of 0.1–1.0% quality percentage [1].

In recent years, increasing attention has been paid to simulation technology in studying the process of MD. Ding et al. [2] developed a mathematical model for hollow fiber components used for MD and analyzed the effect of channel flow in the components using simulated calculation results. The model is used for the macro-transfer process of the membrane. Using the finite element method, Alklaibi [3–5] numerically simulated air gap membrane distillation and direct contact membrane distillation (DCMD) and studied

*Corresponding author.

thermal fluid, cold fluid flow, and the mass transfer resistance. However, the boundary condition was not given. Liu et al. [6] simulated the structure and dynamic behavior of water in limited hydrophobic micro pores by a molecular dynamics method. Self-diffusion coefficient was investigated and analyzed. The performance of separation was not investigated. Ding et al. [7] investigated the performance of a large flat multilayer membrane module used in typical MD systems by using numerical simulation. The mathematical model was built and solved simultaneous equations of other apparatus. The simulation is used for MD systems other than single module. Zhu et al. [8] established a microscopic mass transfer and heat transfer model for vacuum membrane distillation (VMD). The flow in the module was supposed to laminar flow, simulated the experimental data reported in the literature and obtained satisfactory results. Qtaishat et al. [9] established a heat transfer model for a sodium chloride solution submitted to DCMD, solved the heat transfer equations by using the FSOLVE function in the MATLAB software program, and discussed the mass transfer mechanism of a MD process featuring a PTFE membrane; the simulated results and the experimental values of the mass transfer coefficient showed good agreement. Zhong et al. [10] studied the non-equilibrium molecular dynamics influenced by an added force during penetration and the effect of the solution on the permeability coefficient. The separation factor of organic steam and a nitrogen gas mixture passing through a porous carbon membrane was established, and the permeability performance of two types of mixtures, methane/nitrogen (CH_4/N_2) and acetone/nitrogen (CH_3COCH_3/N_2), passing through a carbon membrane were calculated. Using a dusty gas model, Pan et al. [11] established mass transfer and heat transfer mechanism models for the treatment of sodium chloride solution using VMD. Additionally, the researchers effectively incorporated pore size distribution into their MD mechanism model by using the distribution function of the membrane pore size instead of the average diameter. Above all, they mainly focused on separation performance, developing mass transfer and heat transfer models for the process of MD, but they were not concerned with the phenomena observed in the membrane pore; they neither simulated the flow characteristics of the fluid nor the change in the flow field in the membrane pore.

To explore the flow characteristics in membrane pores and improve the process of membrane separation, numerical simulation technology is used to investigate the flow and transfer characteristics in a membrane pore by the treatment of an ethyl acetate solution using VMD. The flow field in the membrane pore is simulated, and the influence of membrane structure parameters on membrane performance is analyzed. The results may be used to enhance the transfer process and guide membrane preparation.

2. Simulation in the membrane pore

2.1. Geometric model

Hydrophobic microporous membranes are used in VMD. In the feed side, the membrane surface contacts the liquid feed directly; part of the volatile components and water gasify and then go into the membrane pore. The pressure on the cold side is lower than the equilibrium vapor pressure of the volatile components on the hot side. With this pressure difference as the driving force, vapor through the membrane pore is sucked into the cold side. The feed solution in the membrane module process during VMD is shown in Fig. 1. A geometric model of a membrane pore is presented in Fig. 2.

2.2. Equations

The flow pattern of vapor moving through a membrane pore is related to the pore structure and vapor density. The Knudsen number (Kn) is an important parameter in micro-scale flow that is determined by the mean free path of gas molecular motion and membrane pore size:

$$\mathrm{Kn} = \lambda/d \tag{1}$$

The average free path of gas molecular motion can be calculated as follows:

$$\lambda = K_B T \Big/ \sqrt{2}\pi\sigma^2 P \tag{2}$$

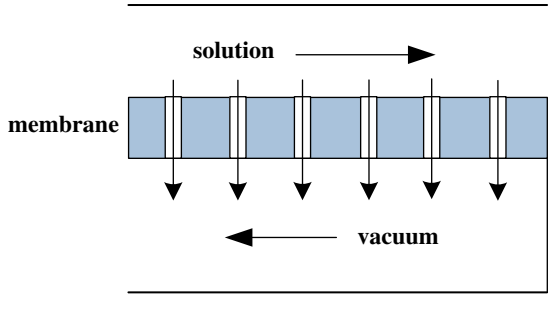

Fig. 1. Feed flow in the membrane module.

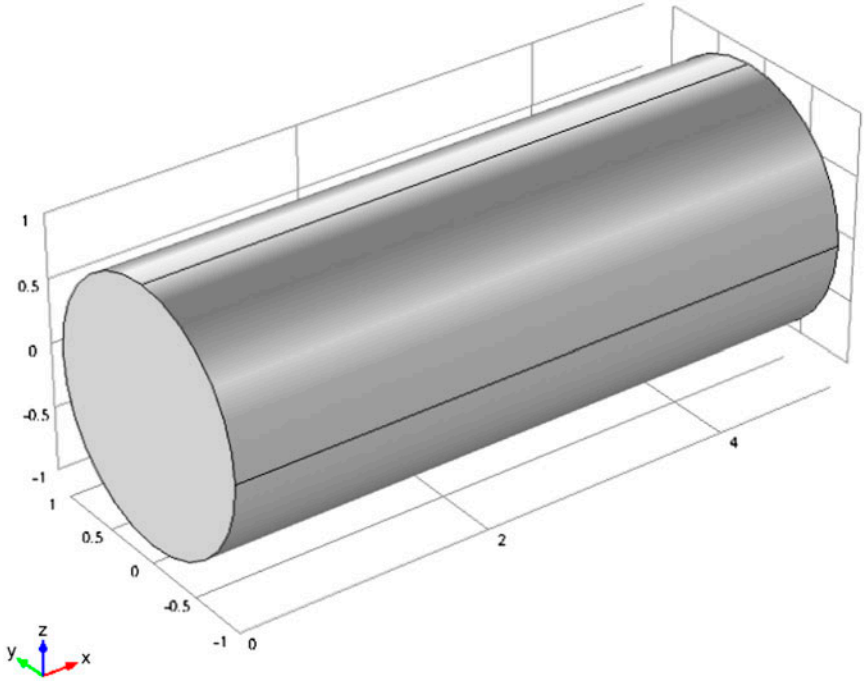

Fig. 2. A geometric model of the membrane pore.

The Kn is used to distinguish the flow pattern in micro-pore flow. According to the Kn, gas flow in a membrane pore is divided into free molecular flow, transitional flow, sliding flow, and continuous medium flow. The value of Kn in membrane pore flow ranges between 10^{-3} and 0.1, which indicates sliding flow [12]. Sliding flow can be described by the Navier–Stokes equations by considering a sliding boundary equation.

The governing equations are the Navier–Stokes equations combined with sliding boundary conditions, including a motion conservation equation, transport conservation equation, and energy conservation equation.

(1) Motion differential equations

$$\rho\frac{D\vec{u}}{Dt} = \rho\vec{F} - \nabla p + \mu\nabla^2\vec{u} + \frac{1}{3}\mu(\nabla\vec{u}) \tag{3}$$

(2) Mass transfer differential equation

$$\rho\nabla\vec{u} + \frac{D\rho}{Dt} = D_{AB}\nabla^2\rho \tag{4}$$

$$\frac{\partial\rho_A}{\partial t} + u_r\frac{\partial\rho_A}{\partial r} + \frac{u_\phi}{r}\frac{\partial\rho_A}{\partial\phi} + u_z\frac{\partial\rho_A}{\partial z} = D_{NA}\left(\frac{1}{r}\frac{\partial}{\partial r}\left(r\frac{\partial\rho_A}{\partial r}\right) + \frac{1}{r^2}\frac{\partial^2\rho_A}{\partial\phi^2} + \frac{\partial^2\rho_A}{\partial z^2}\right) \tag{5}$$

(3) Energy equation

$$\frac{DT}{Dt} = \alpha\nabla^2 T \tag{6}$$

$$\frac{\partial T}{\partial t} + u_r\frac{\partial T}{\partial r} + \frac{u_\phi}{r}\frac{\partial T}{\partial\phi} + u_z\frac{\partial T}{\partial z} = \alpha\left(\frac{1}{r}\frac{\partial}{\partial r}\left(r\frac{\partial T}{\partial r}\right) + \frac{1}{r^2}\frac{\partial^2 T}{\partial\phi^2} + \frac{\partial^2 T}{\partial z^2}\right) \tag{7}$$

(4) Boundary condition

In standard atmospheric conditions, ethyl acetate molecular mean free path is about 0.03 μm. The height of the membrane pore is 0.23 μm. The rate order of magnitude between the average free path of gas molecular motion and the fluid characteristic length

(Kn = λ/L) is 0.1, the flow is the transitional flow. In the micro scale, vapor flow is close to demarcation point between slip stream and transition flow, the Navier–Stokes equation with the sliding boundary [13], the sliding boundary can be described by equation

$$\Delta u_w = \frac{2-\sigma}{\sigma} L_s \left(\frac{\partial u}{\partial y}\right)_w + \frac{3}{4}\frac{\mu}{\rho T}\left(\frac{\partial T}{\partial x}\right)_w \tag{8}$$

Inlet : $c_0 = c_{0,i}, \quad u = u_0, \quad T = T_0;$

Outlet : $P = P_0, \ -n \cdot \vec{N}_i = 0; \ Q = h_m \cdot \Delta T_m.$

2.3. Diffusion coefficient

The membrane pore size and mean free path of molecular motion are of approximately the same order of magnitude; the collisions between molecules and those between molecules and the wall are equally important. The Knudsen diffusion coefficient in a single pore can be expressed as follows:

$$D_{KA} = 48.5 d_p \left(\frac{T}{M_A}\right)^{1/2} \tag{9}$$

The molecular diffusion coefficient of two components can be expressed by Eq. (8):

$$D_{AB} = \frac{1.00 \times 10^{-7} T^{1.75} \left(\frac{1}{M_A} + \frac{1}{M_B}\right)^{1/2}}{P\left[(\sum V_A)^{1/3} + (\sum V_B)^{1/3}\right]^2} \tag{10}$$

The entire diffusion coefficient is expressed as follows:

$$D_{NA} = \frac{1}{\frac{1}{D_{AB}} + \frac{1}{D_{KA}}} \tag{11}$$

In reality, the pores of the membrane are irregular, and the corrected diffusion coefficient is obtained as follows:

$$D'_{NA} = \frac{\varepsilon}{\tau} D_{NA} \tag{12}$$

2.4. Separation performance evaluation

In the VMD process, separation performance is expressed by the membrane permeate flux and separation factor. The flux of MD is calculated by the following formula:

$$J = \frac{m}{At} \tag{13}$$

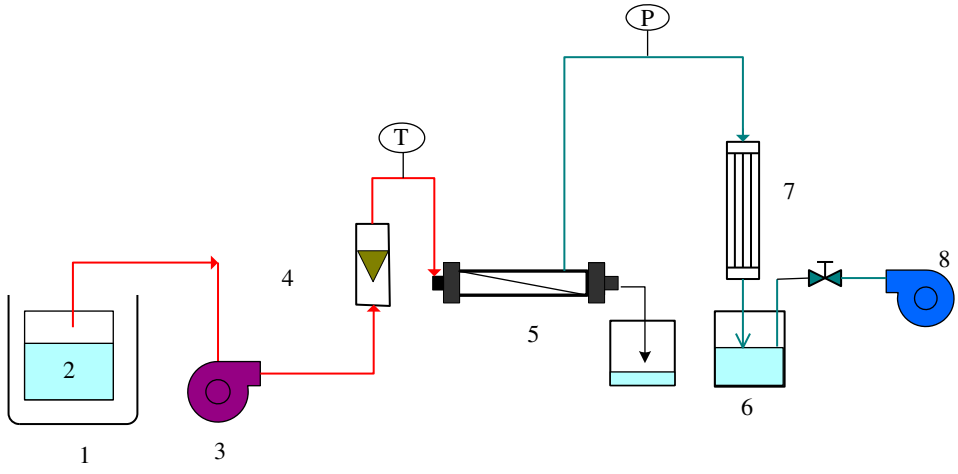

Fig. 3. Experimental setup for VMD: 1 – thermostatic bath; 2 – feed tank; 3 – magnetic driving pump; 4 – rotameter; 5 – membrane module; 6 – distillate receiving flask; 7 – condenser; and 8 – vacuum pump.

Another separation performance parameter is the separation factor, which is calculated as follows:

$$\alpha = \frac{\omega_2(1-\omega_1)}{\omega_1(1-\omega_2)} \tag{14}$$

3. Experiment

The experiment system of VMD apparatus includes heating system, membrane separation system, and condensing collection system, as shown in Fig. 3. The feed ethyl acetate solution in the feed tank is heated in the thermostatic bath and pumped into the membrane module, the mass flow meter is used to measure flow rate. The vapor through the membrane module is collected in the condenser. The membrane flux and separation factor is calculated according to the quality of distillation liquid. Vacuum pump can be set to different vacuum degree. Operating parameters including flow rate, temperature, and vacuum degree can be changed for every measurement. Ethyl acetate solution concentration is measured by spectrophotometer; standard curve is defined to calibrate measured data. Flow rate is measured by flow meter, and temperature and pressure are measured by temperature sensor and pressure sensor, respectively. The heated ethyl acetate solution is pumped by magnetic driving pump. The type and accuracy are shown in Table 1. Thermometer and the temperature are used to calibrate thermostatic bath temperature. The flow meter is calibrated by measuring cylinder. Different concentration of ethyl acetate solution is prepared for measuring absorbance and determining standard curve. When operate parameters are changed, the various water fluxes and separation factors are obtained. The membrane used in experiment is polyvinylidene fluoride hydrophobic membrane.

3.1. Error analysis

Error analysis was performed to understand the sensitivity of these measurements. The error equation are as follows:

$$d = X - \bar{X} \tag{15}$$

$$\phi = d/\bar{X} \tag{16}$$

d was used to indicate the absolute error, ϕ was used to indicate the relative error. After all the data with different temperature were collected, the data from each measurement were analyzed. These data including water flux and separation factor were used to investigate the validity of simulation. The error analysis results concluded that the maximum relative error of water flux was 3%, and the maximum relative error of separation factor was 5%.

4. Results and discussion

4.1. Flow field

The simulation conditions include feed solution concentration, vacuum and feed temperature. The feed concentration of ethyl acetate is 0.14 mol/m^3, the vac-

Table 1
The information of instrument

Instrument	Type	Maker	Calibration standards
Thermostatic bath	HHS-11-2	Shanghai Boxun Company Limited	The temperature range is 37–100℃, calibration standard is 1℃, and the power is 500 W
Magnetic driving pump	MP-15R	Shanghai Xinxishan pump Company Limited	The rated power is 10 W, the rated flow is 16 L/min, and the rated head is 2.4 m
Flow meter	LZB-10	Suzhou chemical instrument Company Limited	The flow measurement range is 10–100 L/h and calibration standard is 0.025
Vacuum pump	SHB-Ⅲ	Zhengzhou Great wall industry and trade Company Limited	The limiting vacuum is 0.098 Mpa and power is 180 W
Pressure sensor	JYB-KO-HAA	Beijing Kunlunhaian Company Limited Sensing Technology Center	Calibration standard is 0.1% FS
Temperature sensor	Pt100 thermal resistance	Xiamen Yudian automation technology Company Limited	Calibration standard is less than 0.015% FS/℃
Spectrophotometer	756PC	Shanghai spectrograph Company Limited	Transmittance is 0.2% T

uum pressure is 0.089 MPa, and the feed temperature is 323 K. The velocity field of the fluid in the membrane pore is shown in Fig. 4. The speed changes from the minimum speed of 0.006 m/s on the wall to the maximum speed of 0.023 m/s, along the axis. Within the same velocity regime, the speed along the axis is the highest; however, the fluid speed is not constant along the axis. The reason is that the collisions between molecules and the wall affect the fluid speed, but the direction of the main body cannot be affected. Considering the influence of the sliding boundary during the simulation process, the speed of the wall is not zero.

The concentration field of ethyl acetate through the membrane pore is shown in Fig. 5. It seems that the concentration of ethyl acetate through the entire length of the membrane pore varies: the growth rate of the ethyl acetate concentration at the entrance is slower than that at the outlet. The concentration of ethyl acetate increases from the minimum 0.14 mol/m^3 at the inlet to the maximum 2.38 mol/m^3 at the outlet.

The driving force for transfer in VMD is the pressure difference between the two sides of pores. The pressure distribution in a membrane pore is shown in Fig. 6. In the simulation, the feed concentration of ethyl acetate is 0.14 mol/m^3, the vacuum pressure is 0.089 MPa, and the feed temperature is 323 K. The pressure changes from 258.47 to 15.44 KPa. Theoretically, the membrane permeate flux is directly proportional to the pressure difference. In actual operation, the selected vacuum pressure should not be higher than the liquid critical pressure through the membrane pore. Otherwise, the liquid in the membrane would prevent separation. The appropriate feeding pressure is near the saturated steam pressure corresponding to the feeding temperature.

To validate the model used in this study, the simulation results are compared with the experimental data. The feed solution is fed at a rate of 76 L/h, the feed concentration is 0.5 wt.%, and the vacuum pressured on the cold side is 89 KPa. The ethyl acetate flux and separation factor are compared, and the results obtained from the numerical simulation and the experimental data are shown in Fig. 7, where the experimental results are represented by the black line and the simulation results are represented by the red line. It can be observed that the trends exhibited by the simulation results are in accordance with that of the experimental results. The average relative error of water flux is less than 12%, the relative error of separation factor is less than 1%. In simulation, all pores are considered to be of the same size and structure; in reality, each pore diameter and tortuosity is different, which leads to slight error.

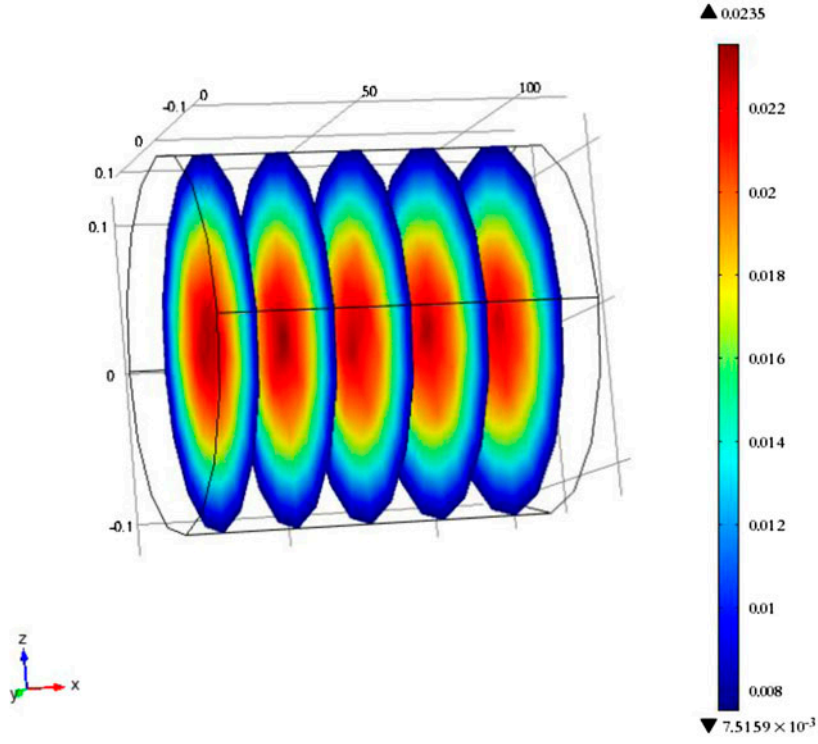

Fig. 4. The velocity field section of the membrane pore.

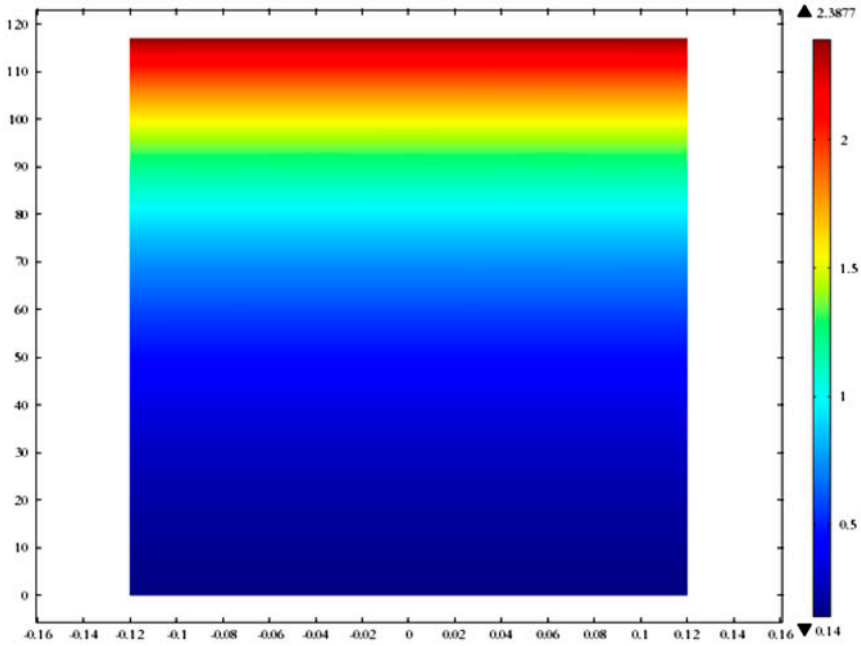

Fig. 5. The concentration field section of ethyl acetate, mol/m^3.

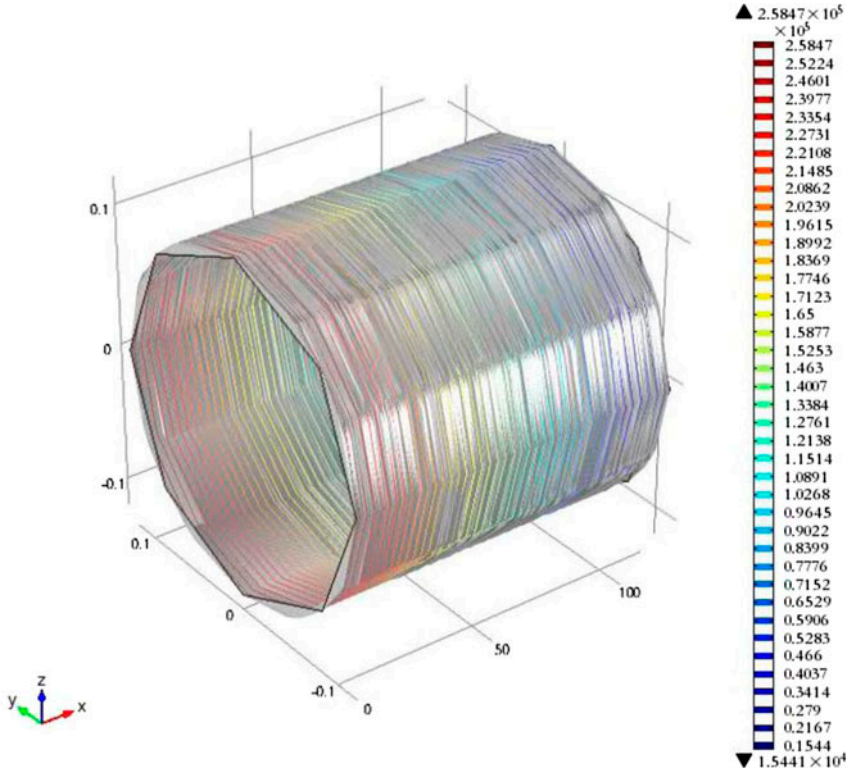

Fig. 6. The pressure distribution of the membrane pore.

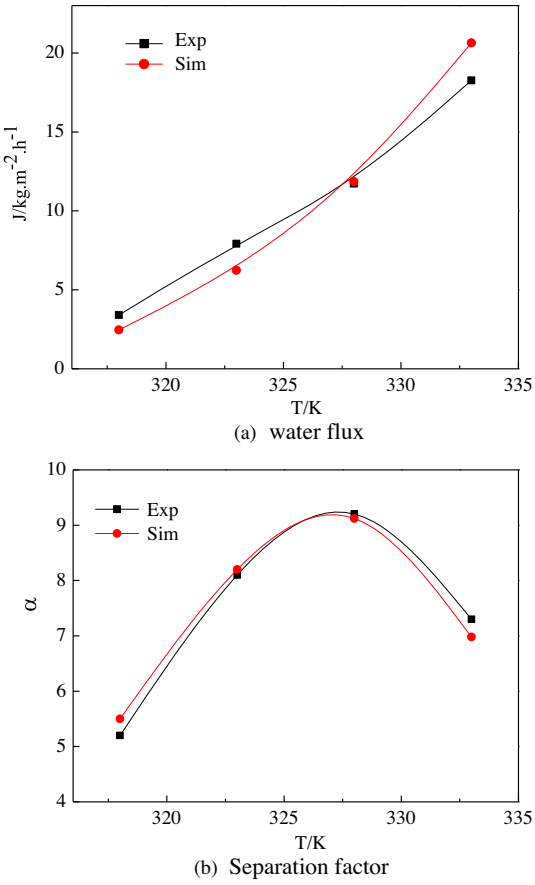

Fig. 7. Comparisons of the experimental and simulation results.

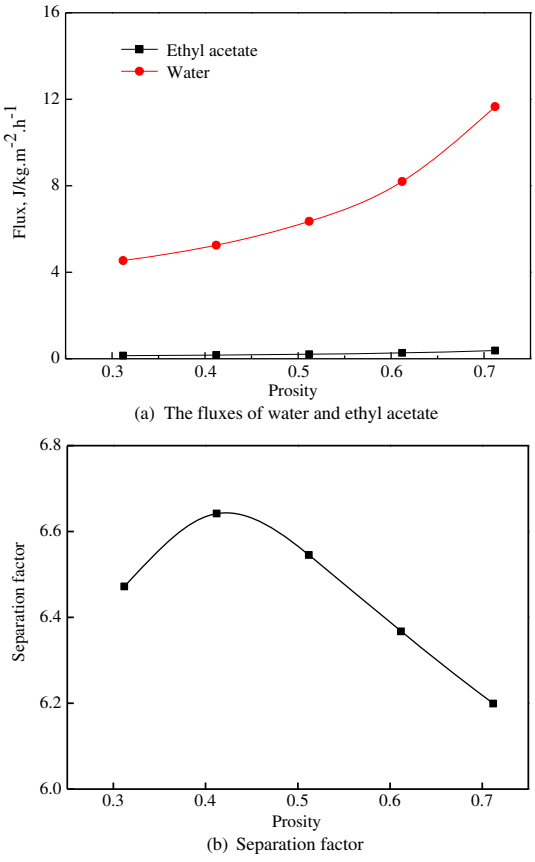

Fig. 8. The effect of porosity on the membrane performance.

4.2. The effect of membrane structure parameters

4.2.1. The effect of porosity

In the simulation process, the tortuosity is set to 6.12, the pore diameter is 0.23 μm, and the length of the membrane pore is 117 μm. The effect of the porosity on the mass transfer diffusion is investigated. As shown in Fig. 8(a), the ethyl acetate flux is represented by the black line and the water flux is represented by the red line. The flux of ethyl acetate and that of water appear to decrease with the increase in porosity. When the membrane porosity changes from 0.31 to 0.71, the ethyl acetate flux increases from 0.14 to 0.38 $kg\,m^{-2}\,h^{-1}$, and the water flux increases from 4.54 to 11.66 $kg\,m^{-2}\,h^{-1}$. The increase in porosity reduces the mass transfer resistance, increases the fluid flow through the membrane per unit time, and leads to an increase in the water and ethyl acetate permeate flux. The effect of the porosity on the separation factor is illustrated in Fig. 8(b). The separation factor increases at first, when the porosity is 0.43, reaches a maximum, and then decreases with the increase in porosity. At first, the velocity of the ethyl acetate solution through the membrane pore is higher than that of the water, and the separation factor increases with the increase in the porosity. Later, the porosity rises to a certain value, and the velocity of the water through the membrane pore is higher than that of the ethyl acetate, which leads to a decrease in the separation factor.

4.2.2. The influence of tortuosity

The simulation porosity is 0.412, the pore diameter is 0.23 μm, and the length of the membrane pore is 117 μm; tortuosity is varied from 2.12 to 8.12. The effect of the tortuosity on the membrane permeate flux is illustrated in Fig. 9(a), where the ethyl acetate flux is represented by the black line and the water flux is represented by the red line. The permeate fluxes of ethyl acetate and water decrease with the increase in the membrane pore tortuosity. The reason why this occurs is that higher tortuosity leads to higher mass

transfer resistance. The effect of tortuosity on the separation performance is illustrated in Fig. 9(b). The separation factors first increase, when the tortuosity is approximately 6.12, reach a maximum, and then decrease with the increase in tortuosity. At first, the separation factor increases with the increase in the tortuosity. When the tortuosity increases further, the separation factor decreases. On a certain scale, with the increase in tortuosity, the collision probability between molecules and the wall is lower than the collision probability between molecules. The water encounters relatively higher mass transfer resistance, and the rate at which the volatile components of ethyl acetate move through the microporous membrane is higher than the velocity of the water; thus, the separation factor increases. With the further increase in the tortuosity, the collision probability between molecules and the wall is higher than the collision probability between molecules; thus, a relatively small pool of ethyl acetate molecule experience higher mass transfer resistance. The rate at which the ethyl acetate moves through the membrane pore decreases, and the separation factor begins to drop.

4.2.3. The influence of pore diameter

The effect of the pore diameter on the mass transfer diffusion is investigated, under the conditions that the porosity is 0.412, the tortuosity is 6.12, and the length of the membrane pore is 117 μm. The pore diameter is varied from 0.2 to 0.8 μm. As shown in Fig 10(a), the membrane permeate flux of the water and ethyl acetate appears to increase with the increase in pore diameter. The ethyl acetate flux increases from 0.19 to 0.47 $kg\,m^{-2}\,h^{-1}$, and the water flux increases from 5.55 to 17.69 $kg\,m^{-2}\,h^{-1}$. The obvious reason for this increase is that the collisions between molecules become more frequent than the collisions between molecules and the pore wall; thus, the increase in the pore diameter reduces gas diffusion resistance, and the membrane permeate flux increases with the increase in pore diameter.

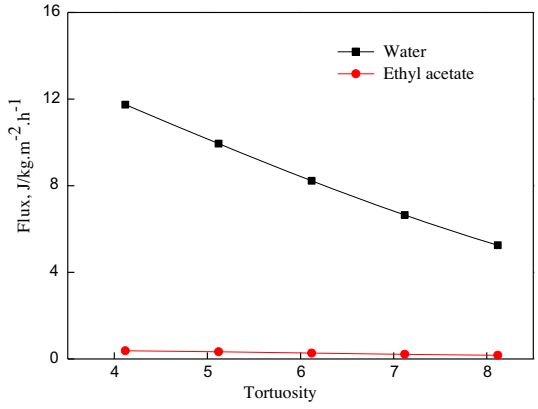

(a) The flux of water and ethyl acetate

(b) Separation factor

Fig. 9. The effect of tortuosity on the membrane performance.

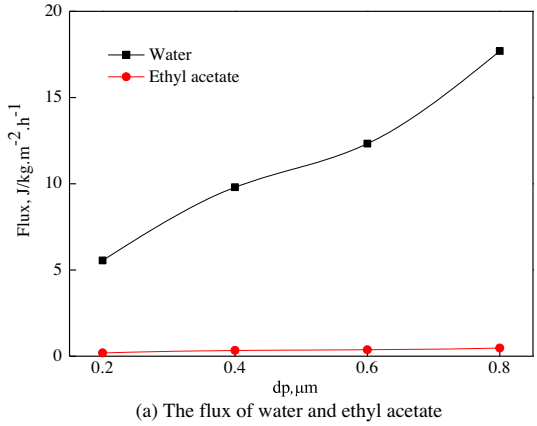

(a) The flux of water and ethyl acetate

(b) Separation factor

Fig. 10. The effect of pore diameter on the membrane performance.

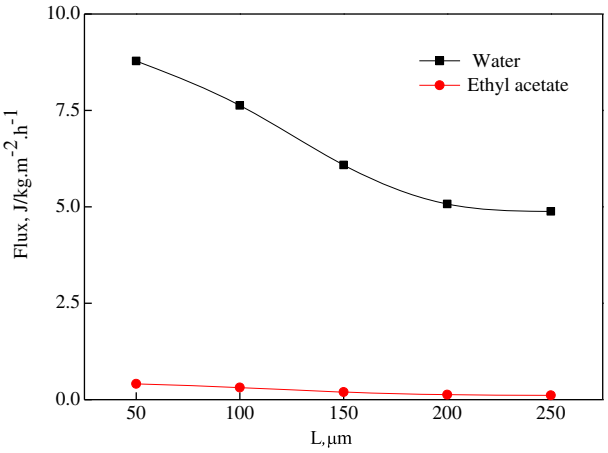

(a) The flux of water and ethyl acetate

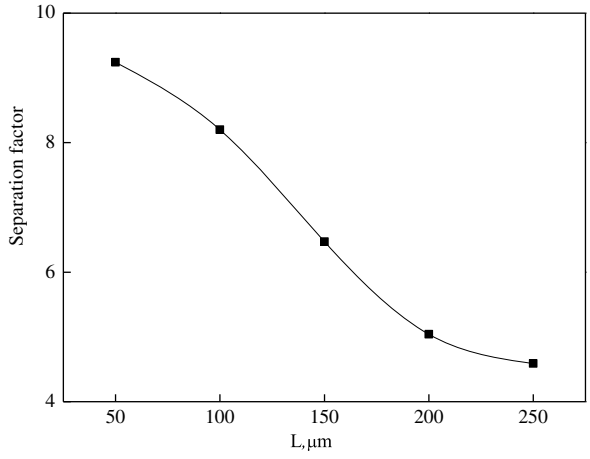

(b) Separation factor

Fig. 11. The effect of pore length on the membrane performance.

Fig. 10(b) shows that the separation factor increases at first, when the pore diameter is approximately 0.6 μm, reaches a maximum of 10.6, and then decreases with the increase in pore diameter. When the pore diameter is in the range of 0.2–0.6 μm, the mass transfer mechanism follows a Knudsen-molecular diffusion mechanism in the membrane pore. When the pore diameter increases further, the permeation rate of water becomes higher than that of the ethyl acetate, and the separation factor begins to decrease.

4.2.4. The influence of the length of membrane pores

The simulations conditions are such that the feed flow rate is 76 L/h, the feed concentration of the ethyl acetate is 0.14 mol/m^3, feed temperature is 323 K, the vacuum pressure is 89 KPa, the porosity is 0.412, the pore diameter is 0.24 μm, and the tortuosity is 6.12. The effects of the pore length on the membrane permeate flux and separation factor are illustrated in Fig. 11. The ethyl acetate flux decreases from 0.4 to 0.12 kg m^{-2} h^{-1}, the water flux decreases from 8.78 to 4.88 kg m^{-2} h^{-1}, and the separation factor decreases from 9.24 to 4.59 when the length of the membrane pore increases from 50 to 250 μm. The reason for this decreasing trend is that the pore length is related to the mass transfer resistance: a longer pore length results in a greater mass transfer resistance. The mass transfer resistance reduces gas permeation, causing the flux to decrease. In the VMD process, thin membranes are chosen to separate mixtures.

5. Conclusions

Using a three-dimensional geometric model, the flow characteristics and transfer characteristics of a membrane pore used to perform VMD to treat ethyl acetate solution are studied, and the flow field in the membrane pore and the effect of the membrane structure parameters on the separation performance are investigated. The results show that the Knudsen and molecular diffusion coefficients for a micro pore are appropriate. Moreover, the simulation results are validated by the experimental data, and the flow field in a membrane pore can be simulated correctly. Different membrane structure parameters may lead to different molecule–molecule and molecule–wall collision probabilities, which result in different membrane performances. The membrane flux increases with the increase in the porosity and pore diameter, and decreases with the increase in the tortuosity and the pore length. The separation factor decreases with the increase in the pore length, and the other membrane structure parameters produce a maximum separation factor value.

Notations

d — the absolute error
X — the measurements
$\overline{X}$ — the average measurements
ϕ — relative error
λ — the average free path of gas molecular motion, m
K_B — Boltzmann constant
η — viscosity coefficient

c_i — i component concentration, mol/m^3
P — the average pressures, Pa
ρ — the fluid density, g/cm^3
∇ — vector differential operator
T — the average temperature in membrane pore, K
σ — the critical diffusion diameter of molecular, m
J — membrane distillation flux, kg/(m^2 h)
m — the quality of sample, kg
A — area of membrane, m^2
t — the sample time, h
α — separation factor
ε — porosity
τ — tortuosity
L — the length of membrane pore, μm
L_s — boundary sliding length, m
$\sum V_i$ — the total atomic volume
N_A — diffusion fluxes, kg/(m^2 h)
ω_1 — the feed concentration by weight
ω_2 — the distillate concentration by weight
$\overline{u}_r$ — the speed in the direction of r, m/s
u_ϕ — the speed in the direction of ϕ, m/s
u_z — the speed in the direction of z, m/s
ρ_A — the density of A, g/cm^3
D_{NA} — diffusion coefficient of A
D_{AB} — molecular diffusion coefficient
D_{KA} — Knudsen diffusion coefficient
M_B — the molecular mass of material B, g/mol
d_p — the diameter of the pore, μm
M_A — the molecular mass of material A, g/mol
$\underline{K}_B$ — Boltzmann constant
F — the quality force of the micro volume
Q — heat flux, (W/m^2)
h_m — heat transfer coefficient, (W/m^2 K)
ΔT_m — mean temperature difference, K

Acknowledgments

This study was supported by the National Nature Science Foundation of China (No. 20806008), National Nature Science Foundation of China (21111120074) and the Foundation of Beijing Key Laboratory for Chemical Power Source and Green Catalysis (2013CX02031).

References

[1] X.Q. Wang, Y.M. Ma, M.D. Wang, The application of membrane distillation technique to water treatment, Ind. Water Treat. 28 (2008) 18–24.
[2] Z.W. Ding, X.D. Chen, R.Y. Ma, Study on the channelling effect in hollow fiber module applied in membrane distillation by numerical simulation, Comput. Appl. Chem. 18 (2001) 499–504.
[3] A.M. Alklaibi, N. Lior, Membrane-distillation desalination: Status and potential, Desalination 171 (2004) 111–131.
[4] A.M. Alklaibi, N. Lior, Transport analysis of air-gap membrane distillation, J. Membr. Sci. 255 (2005) 239–253.
[5] A.M. Alklaibi, N. Lior, Heat and mass transfer resistance analysis of membrane distillation, J. Membr. Sci. 282 (2006) 362–369.
[6] Y.C. Liu, Q. Wang, L.H. Lv, Structural and diffusion properties of water in hydrophobic micropores by molecular simulation, J. Phys. Chem. 21 (2005) 63–68.
[7] Z.W. Ding, L.Y. Liu, W. Liu, Study on the performance of large-scale flat sheet membrane module used in membrane distillation by numerical simulation, Comput. Appl. Chem. 22 (2005) 577–581.
[8] C.Y. Zhu, Z. Gao, X.Q. Gao, Simulation and calculation of membrane parameters in vacuum membrane distillation, Chem. Eng. 34 (2006) 35–38.
[9] M. Qtaishat, T. Matsuura, B. Kruczek, M. Khayet, Heat and mass transfer analysis in direct contact membrane distillation, Desalination 219 (2008) 272–292.
[10] J. Zhong, W. Shao, Q. Xia, Molecular dynamics simulation of organic vapor permeation through carbon membranes, Nat. Gas Chem. Ind. 33 (2008) 24–28.
[11] Y.Q. Pan, Y.L. Yu, F.C. Xu, Research on simulation of desalination of NaCl aqueous solution by vacuum membrane distillation, J. Dalian Univ. Technol. 50 (2010) 328–333.
[12] R.K. Agarwal, K.Y. Yun, R. Balakrishnan, Beyond Navier–Stokes: Burnett equations for flows in the continuum-transition regime, Phys. Fluids 13 (2001) 3061–3085.
[13] C. Xie, J. Fan, Assessment of second-order velocity-slip boundary conditions of the navier-stokes equations, Chin. J. Theor. Appl. Mech. 39 (2007) 1–6.